Rev.Adv.Mater.Sci. 22(2009) 39-51

MOBILITY OF TRIPLE JUNCTIONS OF GRAIN BOUNDARIES DURING THEIR MIGRATION IN DEFORMED NANOCRYSTALLINE MATERIALS

S.V. Bobylev and I.A. Ovid'ko

Institute of Problems of Mechanical Engineering, Russian Academy of Sciences, Bolshoj 61, Vasil. Ostrov, St. Petersburg, 199178, Russia

Received: June 29, 2009

Abstract. A theoretical model is suggested that describes stress-driven migration of grain boundaries (GBs) and their triple junctions in deformed nanocrystalline ceramics and metals. Within the model, the migration process carries plastic flow and is accompanied by both increase in the GB length and transformations of GB dislocations and disclinations at migrating triple junctions. With these factors taken into account, it is found that geometry of triple junctions strongly influences their mobility characterized by the stress level needed to drive migration of GBs and their triple junctions in deformed nanocrystalline materials.

1. INTRODUCTION

The outstanding mechanical properties of nanocrystalline ceramic and metallic materials are attributed to their specific structural features; see, e.g., [1–12]. In particular, plastic flow processes in nanocrystalline materials are crucially influenced by GBs whose amount is extremely large in these materials. For instance, during plastic deformation, GBs in nanocrystalline materials serve as sources of partial lattice dislocations and twins [13–18] and effectively conduct such deformation modes as GB sliding [19–21], Coble creep [22,23], triple junction diffusional creep [24], and rotational deformation [25–29]. Also, recent experimental observations [20,30–44] and computer simulations [38,45–47] have indicated that stress-driven GB migration and corresponding grain growth processes intensively occur in mechanically loaded nanocrystalline and ultrafine-grained materials. In these experiments and computer simulations, it was found that the GB migration and grain growth processes are driven by high stresses.

Following [3,48,49], the stress-driven GB migration is treated as a special deformation mechanism operating in nanocrystalline materials. A very similar process of the stress-driven GB migration occurs in bicrystals [50–55] (Fig. 1a), but at the stress level much lower than that driving GB migration in nanocrystalline materials (Fig. 1b). For instance, the stress-driven GB migration coupled to shear in Al bicrystals has been observed in experiments at quite small applied stresses (< 1 MPa) [54,55]. In contrast, Gianola et al. [38] observed stress-driven grain growth in nanocrystalline Al films during their plastic deformation at a rather high level of the applied stress. The yield stress was in the range 91–116 MPa, and the ultimate tensile strength was in the range 149–190 MPa [38]. With these and other experiments in this area, the high stress level serves as the specific feature of the stress-driven GB migration in nanocrystalline materials, differentiating it from that in bicrystals (see a discussion in paper [49]).

The crucial factor for the difference in question is the role of triple junctions of GBs as structural

Corresponding author: I.A. Ovid'ko, e-mail: ovidko@def.ipme.ru

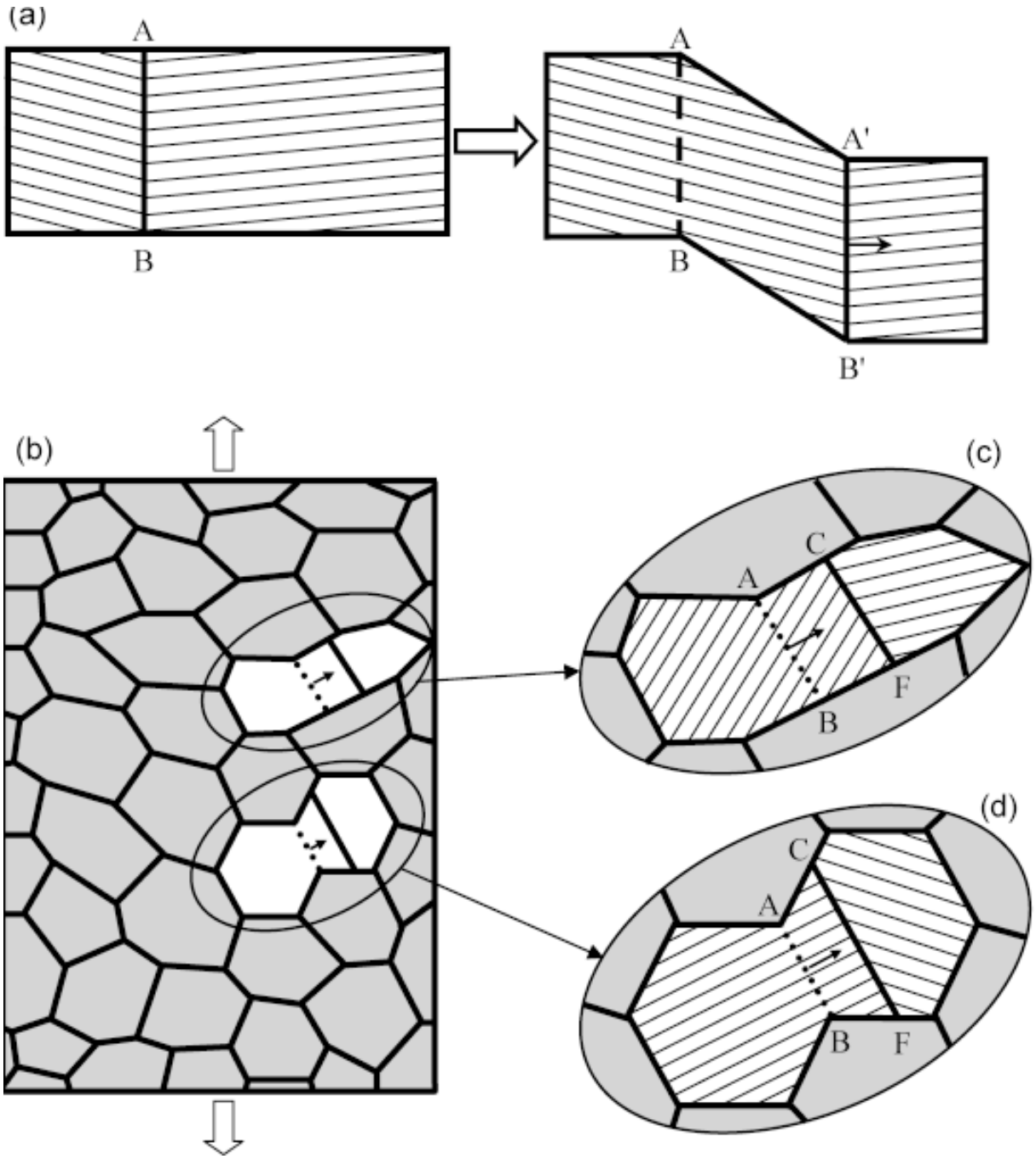

Fig. 1. Stress-driven migration of grain boundaries in (a) bicrystal (where migration of grain boundary from its initial position AB to final position CF is accommodated by change in the bicrystal shape) and (b) nanocrystalline specimen (where the migration process results in plastic flow mismatch between regions traversed by migrating grain boundaries and surrounding material). Magnified insets highlight geometric features of stress-driven migration of grain boundaries in (c) rectangular and (d) hexagonal grains of nanocrystalline specimen.

elements hampering the stress-driven GB migration in nanocrystalline materials [49]. Actually, the shear coupled to GB migration in a bicrystal is easily accommodated by a change of the bicrystal shape (Fig. 1a), in which case the stress needed to initiate the migration process is low. At the same time, the crystal region where the shear coupled to GB migration occurs in a nanocrystalline solid com-

monly represents an internal region in the solid (Fig. 1b), and the shear is strongly hampered by the surrounding material. In this situation, the local plastic shear coupled to the GB migration creates plastic mismatch stresses due to plastic strain/shear incompatibility between the crystal region traversed by the migrating GB and the surrounding material. The flow stress needed to drive GB migration in a nanocrystalline specimen is high, because the flow stress work, in its large part, should be spent to creation of the plastic mismatch stresses, in contrast to the situation with bicrystals (Fig. 1a) in which such plastic mismatch stresses are absent.

From a geometric viewpoint, the plastic mismatch stresses occur at a GB fragment after migration of a triple junction along this fragment. That is, transformations of GB defects at migrating triple junctions determine the flow stress in nanocrystalline materials deformed by the stress-driven GB migration. In Letter [48], the stress-induced GB migration in a nanoscale grain of a nanocrystalline solid was described as a special deformation mode accompanied by formation of wedge disclinations (playing the role of sources of plastic mismatch stresses). Dao with co-workers [3] noted that, for certain ranges of structural parameters (grain size d_{grain} is in the range 10 nm $\leq$ $d_{grain} \leq$ 30 nm, tilt misorientation of migrating GBs is in the range $5° \leq \theta \leq 30°$), the flow stress calculated within the disclination approach [48] as that needed to initiate GB migration is in the prevailing range of experimentally measured stress levels for many nanocrystalline fcc metals.

The disclination approach [48,49] operates with simplified two-dimensional nanocrystalline structures with GBs migrating within rectangular grains (Figs. 1b and 1c). In general, two-dimensional models of nanocrystalline materials are rather conventional and effective in description of plastic flow and GB migration processes in these materials; see, e.g., [56] and references therein. (Many researchers exploit two-dimensional models, because of the three following reasons. First, the analysis of real three-dimensional nanoscale grain structures requires the knowledge of too many factors and parameters, which can hardly be taken into an analytical consideration. Second, plastic deformation mechanisms are directly identified by ("in situ") transmission electron microscopy experiments which commonly deal with nanocrystalline films having two-dimensional-like columnar structures. Third, numerous experiments showed high similarity between the deformation behaviors of nanocrystalline bulk materials and films; see, e.g., the book [56] and references therein.) At the same time, rectangular shape of grains is rarely observed in real materials at their surfaces. A commonly used theoretical description operates with two-dimensional nanocrystalline structures consisting of closely packed hexagonal grains and serving as good models for columnar nanoscale structures of films and first-approximation models for bulk nanocrystalline materials. The main aim of this paper is to elaborate a theoretical description of stress-driven migration of GBs and their triple junctions in deformed nanocrystalline materials in the framework of the "standard model approach" operating with GBs that migrate within hexagonal grains in two-dimensional nanocrystalline structures (Figs. 1b and 1d). A special attention will be paid to sensitivity of triple junction mobility (characterized by the stress needed to drive migration of GBs and their triple junctions) to geometry of triple junctions in deformed nanocrystalline materials.

2. GEOMETRY OF STRESS-DRIVEN MIGRATION OF GRAIN BOUNDARIES AND THEIR TRIPLE JUNCTIONS IN HEXAGONAL NANOGRAIN

Let us describe theoretically GB migration in nanocrystalline materials in the framework of the "standard model approach" operating with GBs that migrate within hexagonal grains in two-dimensional nanocrystalline structures (Figs. 1b and 1d). In doing so, we consider evolution of a typical GB configuration consisting of five GBs, as shown in Fig. 2. For simplicity, we assume that all the GBs are symmetric tilt boundaries. Within our model, in spirit of the continuum dislocation description [57–59] of GB structures in solids, the symmetric tilt GBs (Fig. 2) are modeled as continuous distributions of edge dislocations with infinitesimal Burgers vectors perpendicular to GB planes. Each GB of finite length is characterized by its sum Burgers vector defined as the sum (integral) of infinitesimal Burgers vectors of its continuously distributed dislocations. In the initial configuration (Fig. 2a), triple junctions A and B of GBs are supposed to be compensated, that is, defect-free. In order to minimize the number of parameters of the problem and simplify its analysis, we suppose that GBs I, III and V have the tilt misorientation θ, while GBs II and IV are characterized by the tilt misorientation -2θ (in this case, the sign "minus" means that the misorientation of GBs II and IV is opposite to the

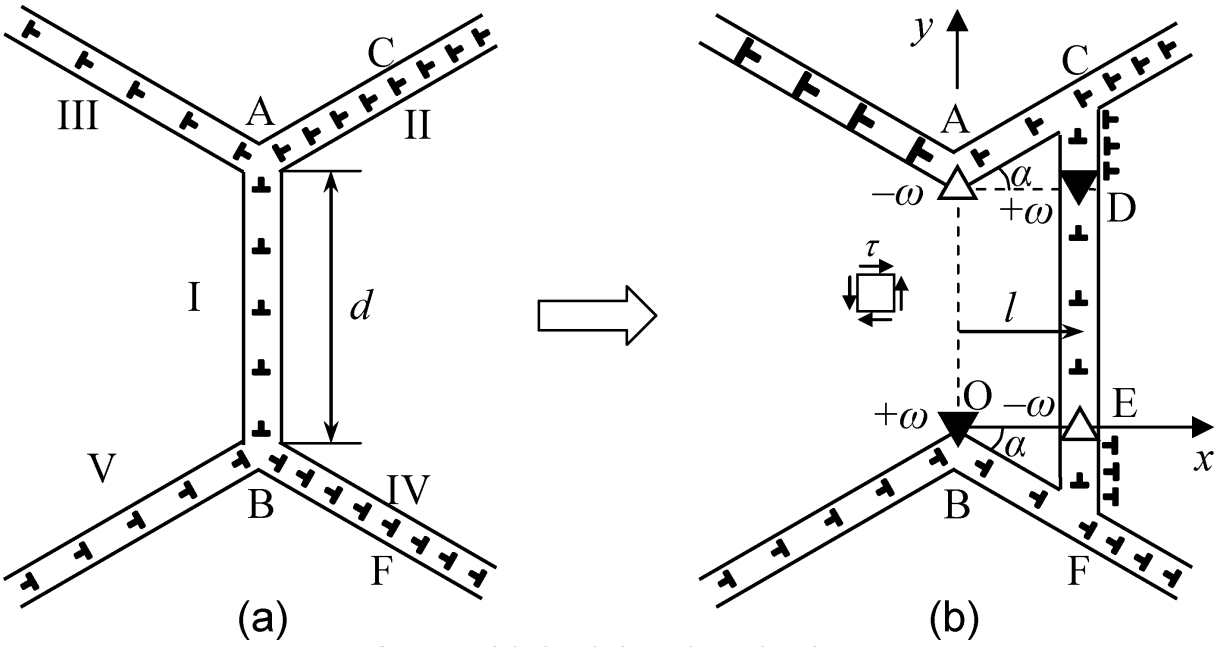

Fig. 2. Model of grain boundary migration.

misorientation of GBs I, III and V). We consider the GB AB which migrates under the action of the shear stress τ over the distance l. As a result of this migration, the migrating GB elongates. More precisely, the length of the GB in its initial position AB is d, while length of the GB in its final position CF is $d + 2l\tan\alpha$, where α is the angle between GB plane II and normal to GB plane I (Fig. 2b). In the context discussed, the angle α serves as an important geometric parameter characterizing both triple junction and its influence on the GB migration under consideration.

Also, let us make the following model assumptions. (1) Misorientation θ of the GB fragment DE during the migration process does not change. (2) New fragments CD and EF of the GB are formed due to splitting of fragments AC and BF of the GBs II and IV, respectively. (Note that, due to symmetry of the system shown in Fig. 2, it is sufficient to analyze the splitting of the GB fragment AC, resulting in formation of the GB fragment CD. The GB fragments BF and EF behave in the same way.) (3) During migration, the sum GB dislocation density (the sum Burgers vector) of all the GBs involved in the migration process does not change. (The latter, in particular, means that the GBs neither absorb lattice dislocations from outside nor emit dislocations to the surrounding material.) The assumptions (1)-(3) will allow us to simplify a mathematical analysis of the stress-driven migration of GBs and their triple junctions in nanocrystalline materials. At the same time, this simplified description definitely reflects the key aspects of the problem under our study.

In the initial configuration, the fragment AC of the GB II is characterized by the length $l/\cos\alpha$ and the tilt misorientation -2θ. As with other GBs in their initial states (Fig. 2a), the fragment AC of the GB II represents a tilt boundary fragment described within our model as a continuous distribution of edge dislocations with infinitesimal Burgers vectors perpendicular to the corresponding GB planes. In doing so, the GB fragment AC is characterized by the sum Burgers vector $\mathbf{B}_0^{AC}$ having both the magnitude $B_0^{AC} = 2\theta l/\cos\alpha$ (in accordance with Frank formula [59,60]) and orientation perpendicular to the GB II plane. Let the new GB CD (resulted from the splitting) be characterized by the sum Burgers vector $\mathbf{B}^{CD}$ assumed to be arbitrary. Thus, in the light of the above model assumption, the GB fragment AC, after the splitting, is characterized by the Burgers vector $\mathbf{B}^{AC} = \mathbf{B}_0^{AC} - \mathbf{B}^{CD}$, having the following projections B_x^{AC} and B_y^{AC} on the coordinate axes Ox and Oy, respectively:

$$B_x^{AC} = B_0^{AC}\sin\alpha - B_x^{CD} = 2\theta l\tan\alpha - B_x^{CD},$$
$$B_y^{AC} = -B_0^{AC}\cos\alpha - B_y^{CD} = -2\theta l - B_y^{CD}. \qquad (1)$$

Here B_x^{AC} and B_y^{AC} are the projections of the vector $\mathbf{B}^{CD}$ on the coordinate axes *Ox* and *Oy*, respectively.

It is more convenient to operate with projections of the considered vectors on both the GB plane and normal to this plane. These projections are in the following relationships with the projections B_x^{AC} and B_y^{AC}:

$$\begin{aligned} &B_{\parallel}^{CD} = B_y^{CD},\ B_{\perp}^{CD} = B_x^{CD}, \\ &B_{\parallel}^{AC} = B_x^{AC}\cos\alpha + B_y^{AC}\sin\alpha = \\ &-B_{\perp}^{CD}\cos\alpha - B_{\parallel}^{CD}\sin\alpha, \\ &B_{\perp}^{AC} = B_x^{AC}\sin\alpha - B_y^{AC}\cos\alpha = \\ &2\theta l\left(\tan\alpha\sin\alpha+\cos\alpha\right)-B_{\perp}^{CD}\sin\alpha+B_{\parallel}^{CD}\cos\alpha. \end{aligned} \tag{2}$$

Here indices || and ⊥ denote projections on the GB plane and on normal to the GB plane, respectively. The positive direction of the component $B_{\parallel}^{AC}$ is chosen as the direction from A towards C. The positive direction of the component $B_{\perp}^{AC}$ is that of the Burgers vector of the GB II in the initial state (Fig. 2a). The Burgers vector perpendicular to the GB plane specifies the GB misorientation in accordance with Frank formula:

$$\begin{aligned} &\theta_{AC} = \frac{B_{\perp}^{AC}}{l/\cos\alpha} = 2\theta - \\ &\frac{\cos\alpha}{l}\left(B_{\perp}^{CD}\sin\alpha - B_{\parallel}^{CD}\cos\alpha\right), \\ &\theta_{CD} = \frac{B_{\perp}^{CD}}{l\tan\alpha}. \end{aligned} \tag{3}$$

Following the dislocation description [59] of GB structures in solids, the Burgers vector parallel with the GB plane specifies both the GB asymmetry and its role as a source of long-range stresses (which essentially increase the energy of the system under consideration).

From formulas (3) it is evident that, in general, the misorientation angles of the GBs AC and CD (Fig. 2b) are different from the initial misorientation angles of the GBs I–III (Fig. 2a). With this difference taken into account, the sum of the misorientation angles of the GBs which join at junctions A, C, and D (and, in the light of symmetry, at junctions B, E, and F), generally speaking, is nonzero. That is, these GB junctions are uncompensated. Each of these GB junctions contains a wedge disclination whose strength is equal to the sum of the misorientation angles of the GBs which join at the junction. Taking into account both the summation rule [61] for misorientation angles of GBs joining at a triple junction and the fact that the misorientation angle magnitudes of the initial GBs are given as: $\theta_I = \theta_{III} = \theta_V = \theta$ and $\theta_{II} = \theta_{IV} = 2\theta$, the strengths of wedge disclinations formed at GB junctions A, B, C, D, E and F during the migration process (Fig. 2) obey the following formulas:

$$\begin{aligned} &\omega_A = -\omega_B = \theta_{III} - \theta_{AC} = \\ &-\theta + \frac{\cos\alpha}{l}\left(B_{\perp}^{CD}\sin\alpha - B_{\parallel}^{CD}\cos\alpha\right), \\ &\omega_C = -\omega_F = \theta_{AC} + \theta_{CD} - \theta_{II} = \\ &\frac{\cos\alpha}{l}\left(B_{\perp}^{CD}\cot\alpha - B_{\parallel}^{CD}\right), \\ &\omega_D = -\omega_E = \theta_I - \theta_{CD} = \theta - \frac{B_{\perp}^{CD}}{l\tan\alpha}. \end{aligned} \tag{4}$$

Now let us consider a scheme of the splitting realised at $B_{\perp}^{CD} = B_{\perp}^{EF} = \theta l\tan\alpha\sin^2\alpha$, and $B_{\parallel}^{CD} = -B_{\parallel}^{EF} = -\theta l\sin^2\alpha$. In the case of this scheme, triple junctions C and F are compensated ($\omega_C=\omega_F=0$) and, as it is shown by calculations not presented here, the energy of the final configuration (Fig. 2b) is low compared to other potential schemes of the splitting. Also, with formulas (2)–(4), for this scheme, one finds that $\omega_A = -\omega_B = -\omega_D = \omega_E = -\theta\cos^2\alpha$ and $B_{\parallel}^{AC} = 0$. That is, the defect configuration resulted from the migration (Fig. 2) is modeled as the superposition of both a quadrupole of wedge disclinations with the strength magnitudes $\omega = \theta\cos^2\alpha$ and continuous rows of edge dislocations distributed along GB fragments CD and EF (Fig. 2b). Each of the continuous dislocation rows is characterized by the sum Burgers vector which is parallel with the GB plane and has the magnitude $B_{\parallel}^{CD} = -B_{\parallel}^{EF} = -\theta l\sin^2\alpha$.

Thus, within our model, we specified geometry of the defect configuration involved in the migration process in hexagonal nanograins (Fig. 2). This serves as a basis for calculation of energy and stress characteristics of stress-driven migration of GBs and their triple junctions in hexagonal nanograins of deformed nanocrystalline materials (see next section).

3. ENERGY AND STRESS CHARACTERISTICS OF STRESS-DRIVEN MIGRATION OF GRAIN BOUNDARIES AND THEIR TRIPLE JUNCTIONS IN HEXAGONAL NANOGRAIN

Let us calculate the characteristic energy difference ΔW due to the splitting and migration of GBs

(Fig. 2) in the discussed situation where $B_{\perp}^{CD} = B_{\perp}^{EF} = \theta l \tan\alpha \sin^2\alpha$, and $B_{\parallel}^{CD} = -B_{\parallel}^{EF} = -\theta l \sin^2\alpha$. The difference ΔW represents the sum of the six terms:

$$\Delta W = W_q + W_{gb}^{CD} + W_{gb}^{EF} + W_d + W_{int}^{q-d} - A, \qquad (5)$$

where W_q denotes the proper energy of the wedge disclination quadrupole ABDE; W_{gb}^{CD} and W_{gb}^{EF} are the energies of new GB fragments CD and EF, respectively; W_d is the energy of continuous rows of edge dislocations having Burgers vectors parallel with planes of GBs CD and EF (including the energy of the interaction between these rows); W_{int}^{q-d} is the energy that characterizes the interaction between the disclination quadrupole ABDE and the dislocation rows; and A is the external stress τ work spent to migration of the GB CF.

The proper energy of the quadrupole ABDE of wedge disclinations with strengths $\omega = \pm\theta\cos^2\alpha$ can be written in the following form [48]:

$$W_q = \frac{1}{2} D\theta^2 d^2 \cos^4\alpha \left[\left(1 + x^2\right) \ln\left(1 + x^2\right) - x^2 \ln x^2 \right], \qquad (6)$$

where $D = G[2\pi(1 - \nu)]$, G is the shear modulus, ν is the Poisson's ratio, and $x = l/d$. Within our model, each of the energies W_{gb}^{CD} and W_{gb}^{EF} represents the energy of a continuous wall of edge dislocations whose sum Burgers vector has the magnitude $B_{\perp}^{CD} = B_{\perp}^{EF} = \theta l \tan\alpha \sin^2\alpha$ and is perpendicular to the corresponding GB plane. The energy W_{gb}^{CD} ($=W_{gb}^{EF}$) is calculated in the standard way [62] as the work spent to generation of defects in the stress fields of other defects. In doing so, we find:

$$W_{gb}^{CD} = W_{gb}^{EF} = \frac{D\left(B_{\perp}^{CD}\right)^2}{2}\left(\ln\frac{R}{l\tan\alpha} + \frac{1}{2}\right) = \frac{1}{2} D\theta^2 d^2 x^2 \tan^2\alpha \sin^4\alpha \left(\ln\frac{R'\cot\alpha}{x} + \frac{1}{2}\right). \qquad (7)$$

Here R is the screening length for stress fields, and $R'=R/d$. Formula (7) does not take into account the elastic interaction between GB fragments CD and EF, because this interaction is automatically accounted in the "disclination" part of the energy of the system under consideration.

The energy W_d of continuous rows of edge dislocations having Burgers vectors parallel with planes of GBs CD and EF (including the energy of the interaction between these rows) is calculated in the similar way, as with W_{gb}^{CD}. In doing so, we obtain:

$$W_d = \frac{1}{2} D\theta^2 d^2 x^2 \sin^4\alpha \left[-2\ln\left(x\tan\alpha\right) + \frac{\left(1 + x\tan\alpha\right)^2}{x^2\tan^2\alpha} \ln\frac{1 + 2x\tan\alpha}{\left(x\tan\alpha + 1\right)^2} + \frac{3x\tan\alpha + 2}{x\tan\alpha} \ln\left(1 + 2x\tan\alpha\right) + 2 \right]. \qquad (8)$$

In the partial case of a symmetric defect configuration shown in Fig. 2b, the interaction energy W_{int}^{q-d} is equal to 0. It is because stresses created by the disclination quadrupole are symmetric relative to its central axes.

The work A of the external stress τ, spent to migration of GB CF, represents the sum of the two terms: the work spent to movement/migration of the initial GB fragment AB (DE) and the works spent to movement/migration of new GB fragments CD and EF. (Within the continuum dislocation model of GBs, these works are calculated by integration of elementary (infinitesimal) works spent to movement of infinitesimally small GB fragments characterized by infinitesimally small Burgers vector magnitudes db. In these circumstances, the work spent to movement of the GB fragment DE is, in fact, equal to the work spent to movement of an edge superdislocation with Burgers vector B^{DE} (equal to the sum Burgers vector of the GB fragment DE) over the distance l, that is, $A^{DE} = \tau B^{DE} l$. The same method allows one to find the works spent to movement of the GB fragments CD and EF. In doing so, one finds: $A^{CD} = A^{EF} = \tau B_{\perp}^{CD} l/2$. (Note that we consider the symmetric defect configuration whose evolution is shown in Fig. 2. Due to the symmetry, the work spent to migration of the new GB fragment CD is equal to that spent to migration of the new GB fragment EF: $A^{CD} = A^{EF}$). Taking into account that $B^{DE} = \theta d$ and $B_{\perp}^{CD} = \theta l \tan\alpha \sin^2\alpha$, we obtain:

$$A = \tau\theta l\left(d + l\tan\alpha\sin^2\alpha\right) = D\theta^2 d^2 \frac{\tau}{D\theta} x\left(1 + x\tan\alpha\sin^2\alpha\right). \qquad (9)$$

To summarize, we found formulas (6)–(9) allowing one to calculate the energy difference ΔW.

With formulas (6)–(9), we calculated the dependences ΔW (x), for various values of the external stress t as well as the angle $\alpha = \pi/6$ and $\alpha = 0$, see Figs. 3a and 3b, respectively. In our calculations, the screening length R (figuring in formula (7)) was taken as $R = 3d$ (or, in other terms, $R/d = R' = 3$).

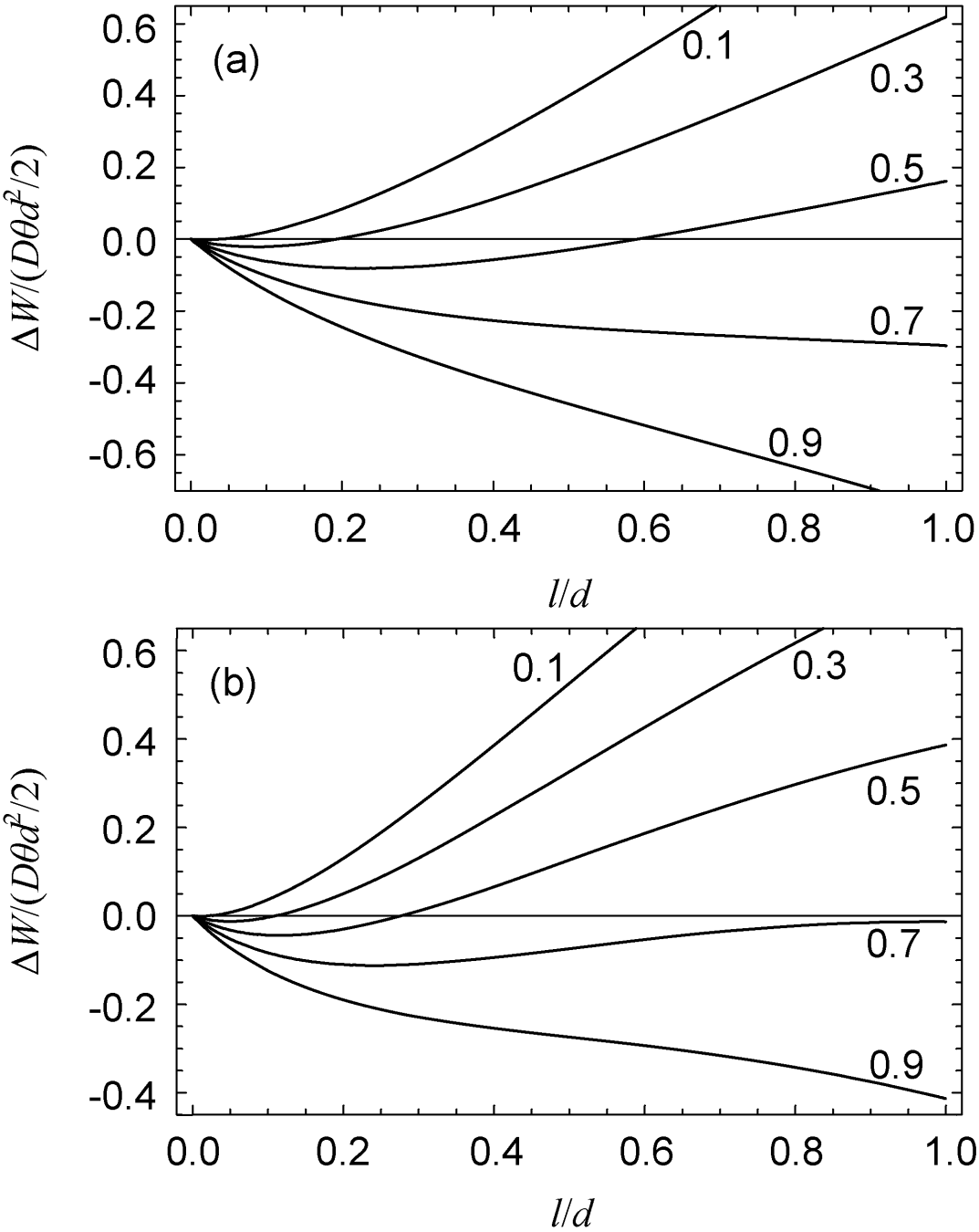

Fig. 3. Dependence of the energy difference ΔW on the migration distance l, for various values of the external stress τ (written in units of $D\theta$) and (a) $\alpha = \pi/6$; and (b) $\alpha = 0$.

From Fig. 3 it is easily seen that, for $x<1$, the dependences $\Delta W(x)$, for $\alpha = \pi/6$ and $\alpha = 0$ (Figs. 3a and 3b, respectively) have similar behaviors, but the energy change ΔW at $\alpha = \pi/6$ is lower than that at $\alpha = 0$. (The dependence $\Delta W(x)$ at $\alpha = 0$ (Fig. 3b) also was calculated in paper [48] describing GB migration in rectangular grains.) That is, the stress-driven GB migration in regular hexagonal grains ($\alpha = \pi/6$) in nanocrystalline materials is more energetically favored than that in rectangular grains ($\alpha = 0$).

In the case of $x>1$, correct calculation of ΔW is impossible within our model. Since the screening length R (figuring in formula (7)) should be signifi-

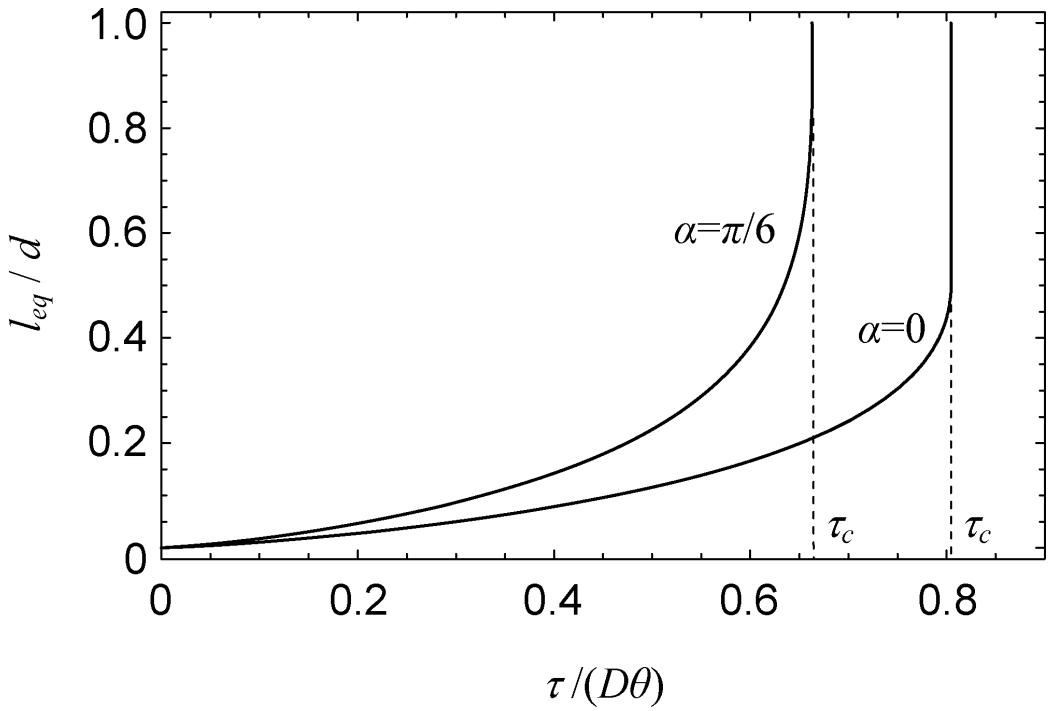

Fig. 4. Dependences of the equilibrium migration distance l_{eq} on the applied stress τ (written in units of $D\theta$), for $\alpha = 0$ and $\alpha = \pi/6$.

cantly larger than l or, in other words, $R/d>>x$, validity of both formula (7) and all the calculation scheme for ΔW may be violated by increasing parameter x. In these circumstances, hereinafter we limit our consideration to the case of $x<1$.

As it follows from Fig. 3, the dependences $\Delta W(x)$ may have minima in the region $x<1$. From the conditions $\partial\Delta W/\partial x = 0$ and $\partial^2\Delta W/\partial x^2 > 0$ one can find the equilibrium distance of stress-driven GB migration $x_{eq}=l_{eq}/d$, where x_{eq} corresponds to the equilibrium minimum at curve $\Delta W(x)$. Fig. 4 presents the dependences $l_{eq}(\tau)$ calculated with the conditions in question, for $\alpha = \pi/6$ and $\alpha = 0$. Dashed lines mark the onset of unstable GB migration at some critical value τ_c of applied stress when minimum of the energy $\Delta W(x)$ disappears. (The unstable migration means that the GB migrates in the non-barrier way until the time moment at which either the migrating GB reaches another GB preventing its movement or a migrating triple junction (located at the migrating GB) reaches another triple junction, in which cases the conditions for further GB migration are not satisfied anymore.) For nanocrystalline Al (with G = 27 GPa and $\nu = 0.34$ [63]), the minimum value (reached at $\alpha \approx 25°$) of the critical stress is $\tau_c \approx 0.35$ GPa, for $\theta = 0.085$ (≈5°), and 1.4 GPa, for $\theta = 0.35$ (≈20°). For nanocrystalline ceramic 3C-SiC (cubic phase of silicon carbide) with G = 217 GPa and $\nu = 0.23$ [64], we get: $\tau_c \approx 2.4$ GPa, for $\theta = 0.085$ (≈5°), and 10 GPa, for $\theta = 0.35$ (≈20°).

Also, we introduce the stress τ_0 needed to drive the experimentally detectable GB migration process. More precisely, τ_0 is the stress at which a GB migrates in the non-barrier way over some small, but experimentally detectable distance l_0. For definiteness, we take l_0 = 3 nm. Fig. 5 presents dependences of τ_0 on the grain size d_{grain} (taken as $d_{grain} = d\sqrt{3}$ for hexagonal grain, where d is the length of the migrating GB) for misorientation values $\theta = 5°$ and 20° in nanocrystalline Al (Fig. 5a) and 3C-SiC (Fig. 5b).

The stress τ_0 is also sensitive to the angle α characterizing triple junction geometry. Within our model, we calculated the dependence of the stress τ_0 (needed to drive GB migration over the distance l_{eq}=3 nm) on α, for nanocrystalline Al and 3C-SiC (see Figs. 6a and 6b, respectively) with various grain sizes d_{grain} = 10,25, and 50 nm. As it follows from Fig. 6, within a certain interval of nonzero angles α, GBs migrate in hexagonal grains more easily (at lower stress level) compared to the pre-

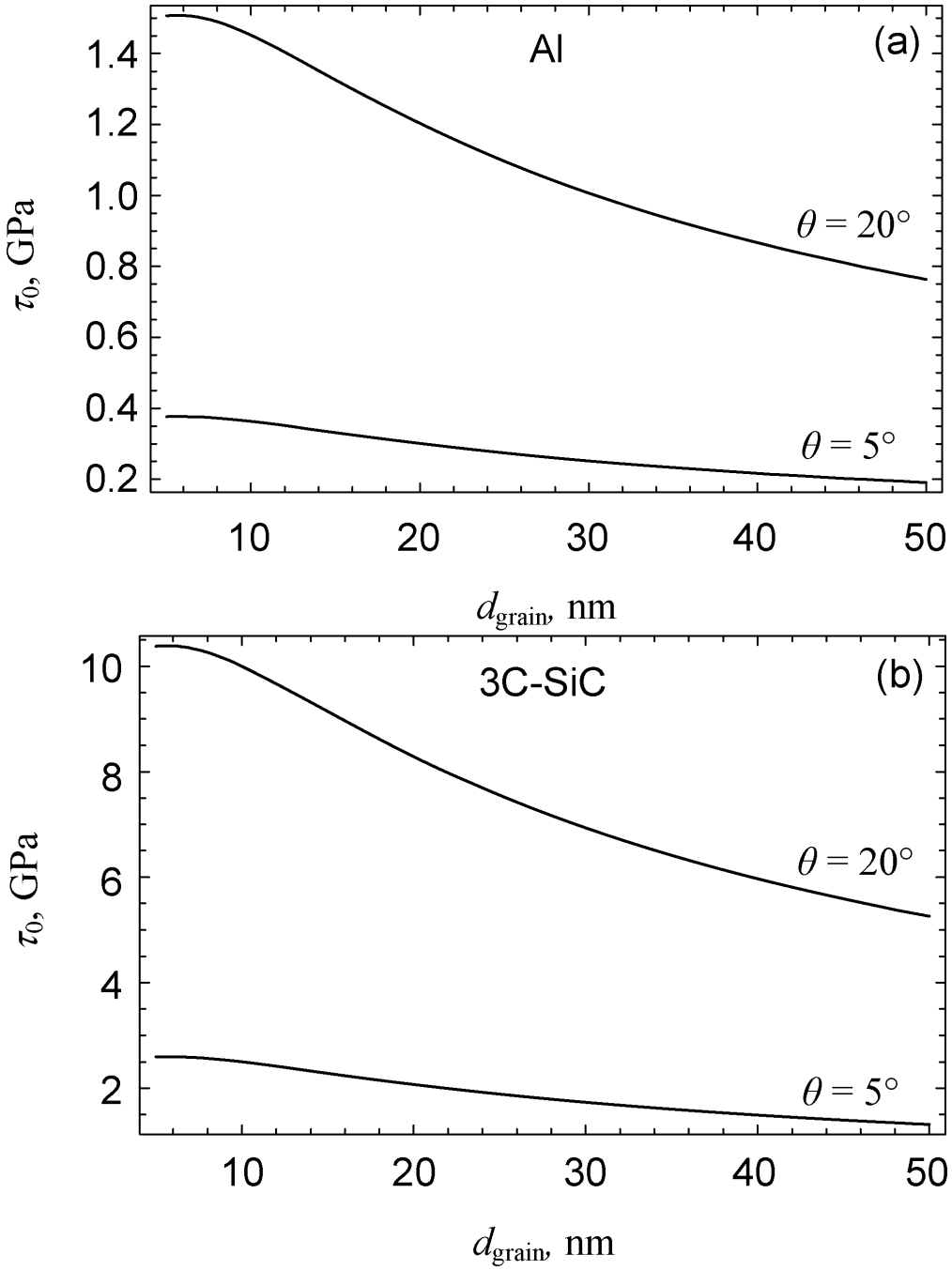

Fig. 5. Dependence of the stress τ_0 needed to drive the grain boundary migration over the distance l_{eq} =3 nm on the grain size d_{grain}, for nanocrystalline (a) Al and (b) 3C-SiC.

viously examined [48] situation with rectangular grains (α = 0). The difference in the stress may reach value of ~20–30% (Fig. 6).

To summarize, the characteristic stress τ_0 (needed to drive GB migration over the distance l_{eq}=3 nm) for the stress-driven GB migration in nanocrystalline materials is highly sensitive to geometric parameters of GBs and their triple junctions involved in the migration process. In particular, τ_0 strongly depends on both the angle α characterizing triple junction geometry and the tilt misorientation parameter θ of a migrating tilt GBs.

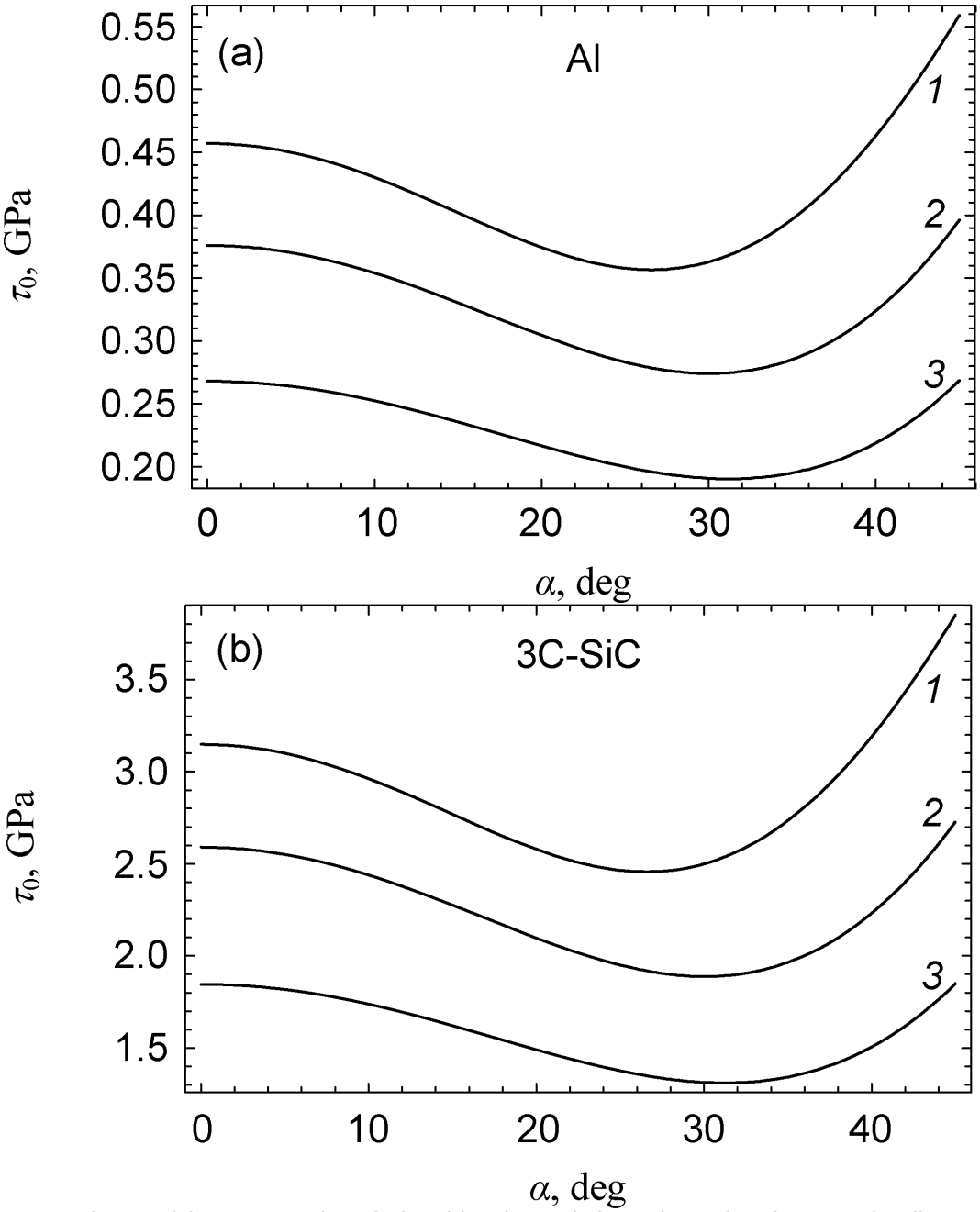

Fig. 6. Dependence of the stress τ_0 (needed to drive the grain boundary migration over the distance l_{eq} = 3 nm) on the angle a (characterizing triple junction geometry), for nanocrystalline (a) Al and (b) 3C-SiC. Curves *1, 2* and *3* correspond to the grain size d_{grain} =10, 25, and 50 nm, respectively.

4. MOBILITY OF TRIPLE JUNCTIONS OF GRAIN BOUNDARIES IN DEFORMED NANOCRYSTALLINE MATERIALS. DISCUSSION

Thus, we have theoretically described the geometric features of stress-driven migration of GBs and their triple junctions in nanocrystalline materials modeled as two-dimensional nanocrystalline structures with hexagonal grains. It was found that the migration process carries plastic flow and is accompanied by increase in the GB length as well as by transformations of GB dislocations and disclinations at migrating triple junctions. All these

factors were taken into account in calculation of energy and stress characteristics of stress-driven migration of GBs and their triple junctions in nanocrystalline metals and ceramics. We found that the stress-driven migration of GBs is energetically favorable within certain ranges of parameters (migration distance l, triple junction angle α) of the system under consideration. Also, geometry of triple junctions crucially influences their mobility and, thus, controls the stress level needed to drive migration of GBs and their triple junctions in nanocrystalline materials. We calculated the dependence of the characteristic shear stress τ (needed to drive the GB migration process) on the equilibrium migration length l_{eq} (Fig. 4) as well as the dependence of the shear stress τ_0 needed to initiate the GB migration (by moving GB over the small, but experimentally detected distance l_{eq} = 3 nm) on grain size d_{grain} (Fig. 5). Following our calculations in the case of nanocrystalline Al with the grain size ~10 nm, typical values of τ_0 (Fig. 5a) range from 300 to 1400 MPa, when misorientation angles are in the range $5° < \theta < 20°$. Molecular dynamics simulations [65] showed similar stress values (~700 MPa) needed to drive GB migration in nanocrystalline Al with the mean grain size 7 nm. These characteristic stress values obtained in molecular dynamics simulations [65] and our theoretical estimates are higher than the experimentally measured [38] values (~50-100 MPa) of the applied shear stress at which stress-driven GB migration and grain growth were observed in nanocrystalline Al films during their plastic deformation. This discrepancy can be related to the occurrence of thermally activated processes and operation of additional deformation modes (different from stress-driven GB migration) in nanocrystalline Al films deformed in experiments [38]. This subject is worth being examined in detail in the future.

Also, we found that, within a certain interval of nonzero angles α, GBs migrate in hexagonal grains more easily (at lower stress level) compared to the previously examined [48] situation with rectangular grains ($\alpha = 0$) (see Fig. 6). The difference in the stress may reach value of ~20–30% (Fig. 6).

Thus, geometry of triple junctions crucially influences their mobility and thereby controls the stress level needed to drive migration of GBs and their triple junctions in deformed nanocrystalline materials. Due to the effects of triple junctions of GBs, this level in nanocrystalline materials is much higher than that in bi-crystals where stress-driven GB migration is freely accommodated by a change of the bicrystal shape.

Finally, note that the reported results are interesting in understanding the specific features of grain growth processes and its sensitivity to tripe junction mobility in nanocrystalline materials under thermal treatment. In particular, these results are important in description of deviations (observed in experiments [66] and computer simulations [67]; see also a short review article [68] and references therein) of grain growth kinetics in nanocrystalline materials from that observed in coarse-grained polycrystals.

ACKNOWLEDGEMENT

This work was supported, in part, by the National Science Foundation Grant CMMI #0700272, the Office of Naval Research (grant N00014-08-1-0405), the Russian Foundation of Basic Research (Grant 08-01-00225-a), and the Russian Academy of Sciences Program “Fundamental studies in nanotechnologies and nanomaterials”.

REFERENCES

[1] D. Wolf, V. Yamakov, S.R. Phillpot, A.K. Mukherjee and H. Gleiter // *Acta Mater.* **53** (2005) 1.

[2] M.A. Meyers, A. Mishra and D.J. Benson // *Progr. Mater. Sci.* **51** (2006) 427.

[3] M. Dao, L. Lu, R.J. Asaro, J.T.M. De Hosson and E. Ma // *Acta Mater*. **55** (2007) 4041.

[4] C.C. Koch, I.A. Ovid’ko, S. Seal and S. Veprek, *Structural Nanocrystalline Materials: Fundamentals and Applications,* (Cambridge University Press, Cambridge, 2007).

[5] H. Klostermann, F. Fietzke, T. Modes and O. Zywitzki // *Rev. Adv. Mater. Sci.* **15** (2007) 33.

[6] M. Balden, C. Adelhelm, T. Köck, A. Herrmann and J. Jaimerena-Muga // *Rev.Adv.Mater.Sci*. **15** (2007) 95.

[7] A. Akbari, J.P. Riviere, C. Templier, E. Le Bourhis and G. Abadias // *Rev. Adv. Mater. Sci*. **15** (2007) 111.

[8] A.M. Saad, V.A. Kalaev, J.A. Fedotova, K.A. Sitnikov, A.V. Sitnikov, Yu.E. Kalinin, A.K. Fedotov and V.A. Svito // *Rev. Adv. Mater. Sci.* **15** (2007) 208.

[9] T. Polcar, A. Nossa, M. Evaristo and A. Cavaleiro // *Rev. Adv. Mater. Sci.* **15** (2007) 118.

[10] I.A. Ovid’ko and A.G. Sheinerman // *Rev.Adv.Mater.Sci*. **16** (2007) 1.

[11] A. Swiderska-Sroda, G. Kalisz, B. Palosz and N. Herlin-Boime // *Rev. Adv. Mater. Sci.* **18** (2008) 422.
[12] T. Yamasaki, H. Yokoyama and T. Fukami // *Rev. Adv. Mater. Sci*. **18** (2008) 711.
[13] M. Chen, E. Ma, K.J. Hemker, H. Sheng, Y. Wang and X. Cheng // Science **300** (2003) 1275.
[14] X.Z. Liao, F. Zhou, E.J. Lavernia, S.G. Srinivasan, M.I. Baskes, D.W. He and Y.T. Zhu // *Appl. Phys. Lett.* **83** (2003) 632.
[15] X.Z. Liao, S.G. Srinivasan, Y.H. Zhao, M.I. Baskes, Y.T. Zhu, F. Zhou, E.J. Lavernia and H.F. Xu // *Appl. Phys. Lett.* **84** (2004) 3564.
[16] Y.T. Zhu, X.R. Liao and R.Z. Valiev // *Appl. Phys. Lett.* **86** (2005) 103112.
[17] M.Yu. Gutkin, I.A. Ovid'ko and N.V. Skiba // *Phys. Rev. B* **74** (2006) 172107.
[18] S.V. Bobylev, M.Yu. Gutkin and I.A. Ovid'ko // *Phys. Rev. B* **73** (2006) 064102.
[19] K. Van Vliet, J. Tsikata and S. Suresh // *Appl. Phys. Lett.* **83** (2003) 1441.
[20] A.K. Mukherjee // *Mater. Sci. Eng. A* **322** (2002) 1.
[21] M.Yu. Gutkin, I.A. Ovid'ko and N.V. Skiba // *Acta Mater.* **52** (2004) 1711.
[22] R.A. Masumura, P.M. Hazzledine and C.S. Pande // *Acta Mater.* **46** (1998) 4527.
[23] V. Yamakov, D. Wolf, S.R. Phillpot and H. Gleiter // *Acta Mater*. **50** (2002) 61.
[24] A.A. Fedorov, M.Yu. Gutkin and I.A. Ovid'ko // *Scripta Mater.* **47** (2002) 51.
[25] M. Murayama, J.M. Howe, H. Hidaka and S. Takaki // *Science* **295** (2002) 2433.
[26] I.A. Ovid'ko // *Science* **295** (2002) 2386.
[27] M.Yu. Gutkin, I.A. Ovid'ko and N.V. Skiba // *Acta Mater*. **51** (2003) 4059.
[28] Zh. Shan, E.A. Stach, J.M.K. Wiezorek, J.A. Knapp, D.M. Follstaedt and S.X. Mao // *Science* **305** (2004) 654.
[29] A.V. Sergueeva and A.K. Mukherjee // *Rev. Adv. Mater. Sci.* **13** (2006) 1.
[30] M. Jin, A.M. Minor, E.A. Stach and J.W. Morris Jr. // *Acta Mater.* **52** (2004) 5381.
[31] W.A. Soer, J.T.M. De Hosson, A. Minor, J.W. Morris Jr. and E. Stach // *Acta Mater*. **52** (2004) 5783.
[32] K. Zhang, J.R. Weertman and J.A. Eastman // *Appl. Phys. Lett.* **85** (2004) 5197.
[33] K. Zhang, J.R. Weertman and J.A. Eastman // *Appl. Phys. Lett.* **87** (2005) 061921.
[34] P.L. Gai, K. Zhang and J.R. Weertman // *Scripta Mater*. **56** (2007) 25.
[35] X.Z. Liao, A.R. Kilmametov, R.Z. Valiev, H. Gao, X. Li, A.K. Mukherjee, J.F. Bingert and Y.T. Zhu // *Appl. Phys. Lett.* **88** (2006) 021909.
[36] D. Pan, T.G. Nieh and M.W. Chen // *Appl. Phys. Lett.* **88** (2006) 161922.
[37] D. Pan, S. Kuwano, T. Fujita and M.W. Chen // *Nano Letters* **7** (2007) 2108.
[38] D.S. Gianola, S. Van Petegem, M. Legros, S. Brandstetter, H. Van Swygenhoven and K.J. Hemker // *Acta Mater.* **54** (2006) 2253.
[39] D.S. Gianola, D.H. Warner, J.F. Molinari and K.J. Hemker // *Scripta Mater*. **55** (2006) 649.
[40] G.J. Fan, L.F. Fu, H. Choo, P.K. Liaw and N.D. Browning // *Acta Mater*. **54** (2006) 4781.
[41] G.J. Fan, Y.D. Wang, L.F. Fu, H. Choo, P.K. Liaw, Y. Ren and N.D. Browning // *Appl. Phys. Lett.* **88** (2006) 171914.
[42] X. Xu, T. Nishimura, N. Hirosaki, R.J. Xie, Y. Yamamoto and H. Tanaka // *Acta Mater*. **54** (2006) 255.
[43] J.T.M. De Hosson, W.A. Soer, A.M. Minor, Z. Shan, E.A. Stach, S.A. Syed Asif and O.L. Warren // *J. Mater. Sci.* **41** (2006) 7704.
[44] W.A. Soer, J.T.M. De Hosson, A.M. Minor, Z. Shan, S.A. Syed Asif and O.L. Warren // *Appl. Phys. Lett.* **90** (2007) 181924.
[45] A.J. Haslam, D. Moldovan, V. Yamakov, D. Wolf, S.R. Phillpot and H. Gleiter // *Acta Mater*. **51** (2003) 2097.
[46] F. Sansoz and V. Dupont // *Appl. Phys. Lett.* **89** (2006) 111901.
[47] D. Farkas, A. Froseth and H. Van Swygenhoven // *Scripta Mater.* **55** (2006) 695.
[48] M.Yu. Gutkin and I.A. Ovid'ko // *Appl. Phys. Lett.* 87 (2005) 251916.
[49] I.A. Ovid'ko, A.G. Sheinerman and E.C. Aifantis // *Acta Mater.* **56** (2008) 2718.
[50] M. Winning, G. Gottstein and L.S. Shvindlerman // *Acta Mater.* **50** (2002) 353.
[51] J.W. Cahn and J.E. Taylor // *Acta Mater.* **52** (2004) 4887.
[52] J.W. Cahn, Y. Mishin and A. Suzuki // *Philos. Mag.* **86** (2006) 3965.
[53] J.W. Cahn, Y. Mishin and A. Suzuki // *Acta Mater.* **54** (2006) 4953.
[54] D.A. Molodov, V.A. Ivanov and G. Gottstein // *Acta Mater.* **55** (2007) 1843.
[55] D.A. Molodov, T. Gorkaya and G. Gottstein // *Mater. Sci. Forum* **558–559** (2007) 927.
[56] I.A. Ovid'ko // *Int. Mater. Rev.* **50** (2005) 65.

[57] B.A. Bilby, In: *Bristol conference report on defects in crystalline materials*, (Physical Society, London, 1955), p. 123.
[58] B.A. Bilby, In: *Progress in solid mechanics, vol. 1*, ed. by I.N. Sneddon and R.P. Hill (Amsterdam: North-Holland; New York: Interscience, 1960), p. 330.
[59] A.P. Sutton and R.W. Balluffi, *Interfaces in Crystalline Materials*, (Clarendon, Oxford, 1995).
[60] A.E. Romanov and V.I. Vladimirov, *Disclinations in crystalline solids*, In: *Dislocations in Solids*, Vol. 9, ed. by F.R.N. Nabarro (North-Holland Publ. Co., Amsterdam, 1992), p. 191.
[61] G.P. Dimitrakopulos, P. Komninou, Th. Karakostas and R.C. Pond // *Interf. Sci.* **7** (1999) 217.
[62] T. Mura, *Micromechanics of Defects in Solids* (Dordrecht: Martinus Nijhoff, 1987).
[63] J.P. Hirth and J. Lothe, *Theory of Dislocations* (Wiley, New York, 1982).
[64] Z. Ding, S. Zhou and Y. Zhao // *Phys. Rev. B* **70** (2004) 184117.
[65] F. Sansoz and V. Dupont // *Appl. Phys. Lett.* **89** (2006) 111901.
[66] G. Krill III, L. Helfen, D. Michels, H. Natter, A. Fitch, O. Masson and R. Birringer // *Phys. Rev. Lett.* **86** (2001) 842.
[67] D. Moldovan, V. Yamakov, D. Wolf and S.R. Phillpot // *Phys. Rev. Lett.* **89** (2002) 206101.
[68] R.A. Masumura and C.S. Pande // *Mater. Sci. Eng. A* **409** (2005) 125.